Temporary and net sinks of atmospheric CO_2 due to chemical weathering in subtropical catchment with mixing carbonate and silicate lithology

Yingjie Cao[a,c,d], Yingxue Xuan[a,b], Changyuan Tang[a,b,c]*, Shuai Guan[e], Yisheng Peng[a,c]

[a]School of Environmental Science and Engineering, Sun Yat-Sen University, Guangzhou, China

[b]School of Geography and Planning, Sun Yat-Sen University, Guangzhou, China

[c]Guangdong Provincial Key Laboratory of Environmental Pollution Control and Remediation Technology, Sun Yat-Sen University, Guangzhou, China

[d]Southern Marine Science and Engineering Guangdong Laboratory, Zhuhai, China

[e]Guangdong Research Institute of Water Resource and Hydropower, Guangzhou, China

Abstract: The study provided the major ion chemistry, chemical weathering rates and temporary and net CO_2 sinks in the Beijiang River, which was characterized as hyperactive region with high chemical weathering rates, carbonate and silicate mixing lithology and abundant sulfuric acid chemical weathering agent of acid deposition and acid mining drainage (AMD) origins. The total chemical weathering rate of 85.46 $t \cdot km^{-2} \cdot a^{-1}$ was comparable to other rivers in the hyperactive zones between the latitude 0-30°. Carbonate weathering rate of 61.15 $t \cdot km^{-2} \cdot a^{-1}$ contributed to about 70% of the total. The lithology, runoff and geomorphology had significant influence on the chemical weathering rate. The proportion of carbonate outcrops had significant positive correlation with the chemical weathering rate. Due to the interaction between dilution and compensation effect, significant positive linear relationship was detected between runoff and total, carbonate and silicate

weathering rates. The geomorphology factors such as catchment area, average slope and hypsometric integral value (HI) had non-linear correlation with chemical weathering rate and showed significant scale effect, which revealed the complexity in chemical weathering processes. DIC-apportionment showed that CCW (Carbonate weathering by CO_2) was the dominant origin of DIC (35%-87%). SCW (Carbonate weathering by H_2SO_4) (3%-15%) and CSW (Silicate weathering by CO_2) (7%-59%) were non-negligible processes. The temporary CO_2 sink was 823.41 10^3 mol km^{-2} a^{-1}. Compared with the "temporary" sink, the net sink of CO_2 for the Beijiang River was approximately 23.18×10^3 mol km^{-2} a^{-1} of CO_2 and was about 2.82% of the "temporary" CO_2 sink. Human activities (sulfur acid deposition and AMD) dramatically decreased the CO_2 net sink and even make chemical weathering a CO_2 source to the atmosphere.

Keywords: Chemical weathering, DIC-apportionment, CO_2 temporary sink, CO_2 net sink

1 Introduction

Chemical weathering driven by weak carbonic acid (H_2CO_3) that originates from atmosphere CO_2 or soil respiration under natural conditions is a fundamental geochemical process regulating the atmosphere-land-ocean carbon fluxes and earth's climate (Guo et al., 2015). Carbonate and silicate weathering define the two typical categories of chemical weathering. From the view of the global carbon cycle, the CO_2 consumption due to carbonate weathering is recognized the "temporary" sink because the flux of CO_2 consumed by carbonate dissolution on the continents is balanced by the flux of CO_2 released into the atmosphere from the oceans by carbonate precipitation on the geological time scale (Cao et al., 2015; Garrels, 1983). While the consumption of CO_2 during the chemical weathering of silicate rocks has been regard as the net sink of CO_2 and regulates the global carbon cycle (Hartmann et al., 2009; Hartmann et al., 2014b; Kempe and Degens, 1985; Lenton and

45 Britton, 2006). Thus in carbonate-silicate mixing catchment, it is essential to distinguish proportions
46 of the two most important lithological groups, i.e., carbonates and silicates, and evaluate the net
47 CO_2 sink due to chemical weathering of silicate (Hartmann et al., 2009).

48 In addition to the chemical weathering induced by H_2CO_3, sulfuric acid (H_2SO_4) of
49 anthropogenic origins produced by sulfide oxidation such as acid deposition caused by fossil fuel
50 burning and acid mining discharge (AMD) also becomes an important chemical weathering agent
51 in the catchment scale. Many studies have shown the importance of sulfide oxidation and subsequent
52 dissolution of other minerals by the resulting sulfuric acid at catchment scale (Hercod et al., 1998;
53 Spence and Telmer, 2005). Depending on the fate of sulfate in the oceans, sulfide oxidation coupled
54 with carbonate dissolution could facilitate a release of CO_2 to the atmosphere (Spence and Telmer,
55 2005), the carbonate weathering by H_2SO_4 plays a very important role in quantifying and validating
56 the ultimate CO_2 consumption rate. Thus, under the influence of human activities, the combination
57 of silicate weathering by H_2CO_3 and carbonate weathering by H_2SO_4 controlled the net sink of
58 atmospheric CO_2.

59 Numerous studies on chemical weathering of larger rivers have been carried out to examine
60 hydrochemical characteristics, chemical erosion and CO_2 consumption rates, and long-term climatic
61 evolution of the Earth, such as the Changjiang River (Chen et al., 2002; Ran et al., 2010), the
62 Huanghe River (Zhang et al., 1995), the Pearl River (Gao et al., 2009; Xu and Liu, 2010; Zhang et
63 al., 2007), the Huai River (Zhang et al., 2011), the rivers of the Qinghai-Tibet Plateau (Jiang et al.,
64 2018; Li et al., 2011; Wu et al., 2008), the Mekong River (Li et al., 2014), the rivers of the Alpine
65 region (Donnini et al., 2016), the Sorocaba River (Fernandes et al., 2016), the rivers of Baltic Sea
66 catchment (Sun et al., 2017), the Amazon River (Gibbs, 1972; Mortatti and Probst, 2003; Stallard

and Edmond, 1981; Stallard and Edmond, 1983; Stallard and Edmond, 1987), the Lena River (Huh and Edmond, 1999) and the Orinoco River (Mora et al., 2010). For simplicity of calculation procedure, most of the researches have ignored the sulfuric acid induced chemical weathering and resulted in an overestimation of CO_2 sink. To overcome this shortcoming of traditional mass-balance method, we applied a dissolved inorganic carbon source (DIC) apportionment procedure to discriminate the contribution of sulfuric acid induced chemical weathering to validate the temporary and net sink of CO_2 in a typical hyperactive region with carbonate-silicate mixing lithology to give a further understanding of basin scale chemical weathering estimation.

About half of the global CO_2 sequestration due to chemical weathering occurs in warm and high runoff regions (Ludwig et al., 1998), so called the hyperactive regions and hotspots (Meybeck et al., 2006). The Pearl River located in the subtropical area in South China includes three principal rivers: the Xijiang, Beijiang, and Dongjiang Rivers. The warm and wet climatic conditions make the Pearl River a hyperactive region in China. The three river basins have distinct geological conditions. The Xijiang River is characterized as the carbonate-dominated area and the Dongjiang River has silicate as the main rock type. While the Beijiang River, which is the second largest tributary of the Pearl River, is characterized as a typical carbonate-silicate mixing basin. In addition, as the serve acid deposition (Larssen et al., 2006) and active mining area (Li et al., 2019), chemical weathering induced by sulfuric acid make the temporary and net sink of atmospheric CO_2 to be reevaluated. So that, in this study, the Beijiang River in Southeast China with a typical subtropical monsoon climate and carbonate-silicate mixing geologic settings was selected as the study area. Three main objectives were summarized as follows: (1) revealed spatial-temporal variations of major element chemistry of the river water, (2) calculated the chemical weathering rate and

unraveled the controlling factors on chemical weathering processes, and (3) determinated the temporary sink of CO_2 and evaluated the influence of sulfide oxidation on net sink of CO_2 by DIC apportionment procedure.

2 Study area

The Beijiang River Basin, which is the second largest tributary of the Pearl River Basin, is located in the southeast of China (Fig. 1). It covers an area of 52 068 km^2 and has a total length of 573 km. The river basin is located in subtropical monsoon climate zone, with the mean annual temperature across the drainage basin ranging from 14°C to 22°C, the mean annual precipitation ranging from 1390 mm to 2475 mm. The average annual runoff is 51 billion m^3, with 70%-80% of the flux occurring from April to September. This can be attributed to the fact that more than 70% of the annual precipitation (about 1800 mm $year^{-1}$) is concentrated in the wet season (April to September).

Lithology in the river basin is composed of limestone, sandstone, gneiss and glutenite. In the upper basin, carbonate rock (mainly of limestone) outcrops in the west and center, while sandstone of Devonian era and mudstone of Paleogene era outcrop in the east of upper stream. In the middle of basin, limestone and sandstone cover most of the area, and Cretaceous volcanic rocks are found in the tributary (Lianjiang River), mainly granite. In the lower basin, Achaen metamorphic rocks outcrop in the west, and are composed of gneiss and schist, sandstone covers rest of area of the lower basin. Quaternary sediments scatter along the main stream of the river. The carbonate and silicate rock outcrops in the Beijiang River Basin was 10737 km^2 (28%) and 24687 km^2 (65%), respectively.

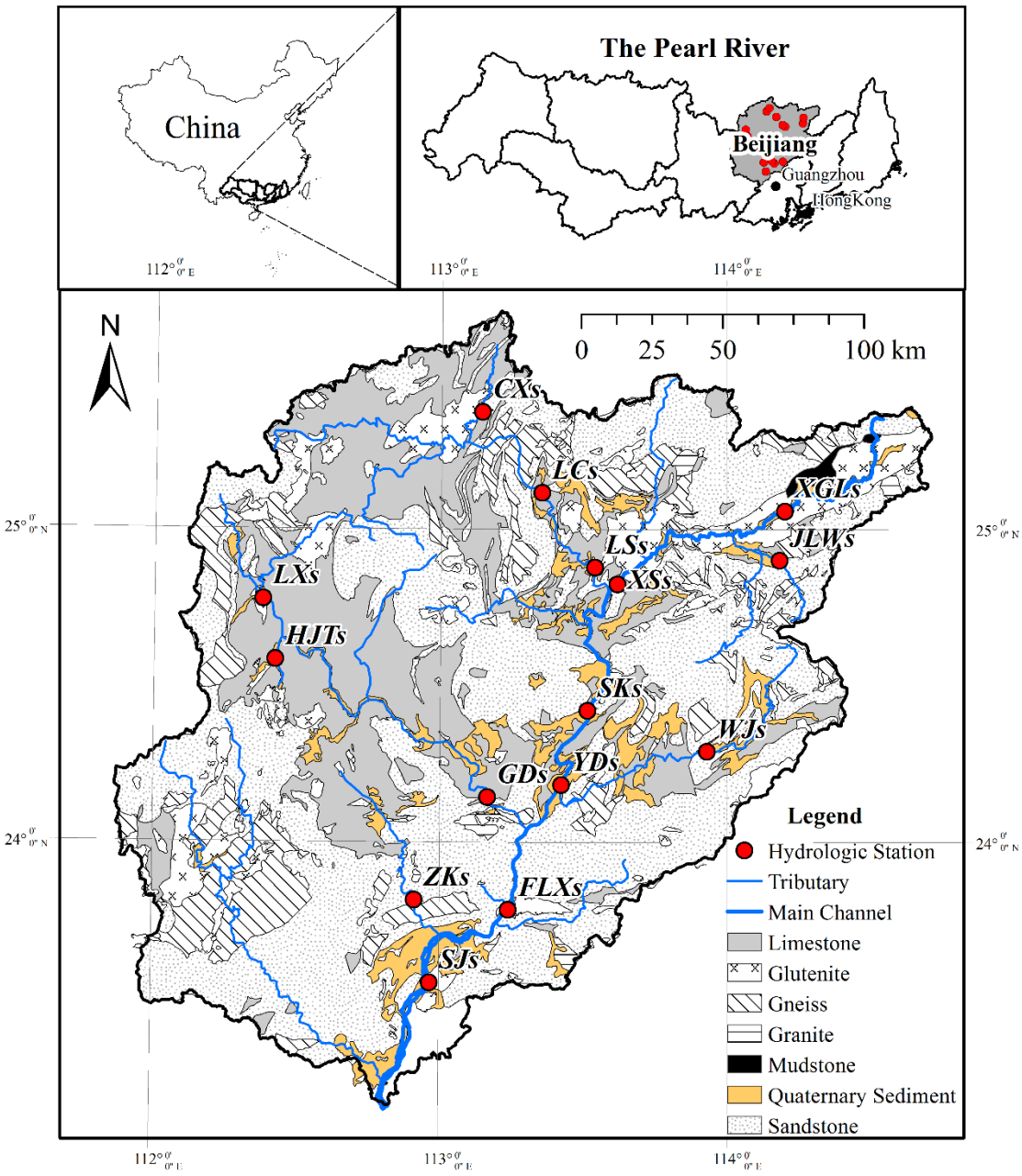

110

111 **Fig. 1 Geology map and sampling point in the Beijiang River basin (produced by Arcgis)**

112 **3 Materials and methods**

113 **3.1 Sampling procedure and laboratory analysis**

114 Water samples were collected monthly at 15 hydrologic stations from January to December in

115 2015 (Fig. 1). The river waters were sampled by a portable organic class water sampler along the

116 middle thread of channel in the first day of each month. In addition, to discriminate the contribution

117 of rain inputs, the daily rainwater was also sampled in five stations (SJs, FLXs, YDs, XSs and XGLs)

along the main stream. The rainwater collector is consisted of a funnel with diameter of 20 cm and a 5 L plastic bottle. A rubber ball is setup in the funnel to prevent evaporation. All the river and rain water were filtered through 0.45 μm glass fiber filter and stored in 100 ml tubes and stored below 4°C until analysis.

Electric conductivity (EC), pH and temperature (T) were measured by a multi-parameter water quality meter (HACH-HQ40Q), and alkalinity (HCO_3^-) was measured in filtered water samples by titration in situ. The dissolved SiO_2 was measured by molybdenum yellow method and was analyzed by ultraviolet spectrophotometer (Shimadzu UV-2600). The cations (Na^+, K^+, Ca^{2+}, Mg^{2+}) and anions (Cl^-, SO_4^{2-}) were analyzed by ion chromatography (ThermoFisher ICS-900) with limit of detection (L.O.D) of 0.01 mg/L. Reference, blank and replicate samples were employed to check the accuracy of all the analysis and the relative standard deviations of all the analysis were within ±5%. The electrical balance (E.B.) defined by the equation of $E.B. = \frac{meq(sum\ of\ cations) - meq(sum\ of\ anions)}{meq(sum\ of\ cations\ and\ anions)} \times 100$ of the water samples was less than 5%.

3.2 Calculation procedure

3.2.1 Chemical weathering rates

The mass balance equation for element *X* in the dissolved load can be expressed as (Galy and France-Lanord, 1999):

$$[X]_{\mathrm{riv}} = [X]_{\mathrm{pre}} + [X]_{\mathrm{eva}} + [X]_{\mathrm{sil}} + [X]_{\mathrm{car}} + [X]_{\mathrm{anth}} \quad (1)$$

Where [*X*] denotes the elements of Ca^{2+}, Mg^{2+}, Na^+, K^+, Cl^-, SO_4^{2-}, HCO_3^- in $mmol \cdot L^{-1}$. The subscripts riv, pre, eva, sil, car and anth denote the river, precipitation source, evaporite source, silicate source, carbonate source and anthropogenic source.

In the study area, the anthropogenic source of major ions except for SO_4^{2-} was ignored due to

the following two reasons. (1) Two main characteristics of much polluted rivers are that TDS is greater than 500 mg/L and the Cl^-/Na^+ molar ratio is greater than that of sea salts (about 1.16) (Cao et al., 2016a; Gaillardet et al., 1999). The TDS in the study area ranged from 73.79 to 230.16 $mg \cdot L^{-1}$ and the low TDS implied that the anthropogenic origins of major ions could be ignored in the study. However, the Beijiang River is characterized as a typical region suffered from serve acid deposition (Larssen et al., 2006) and active mining area (Li et al., 2019). The acid deposition and acid mining discharge contribute to the highest concentration of SO_4^{2-}. (2) Natural origin of SO_4^{2-} is the dissolution of evaporite, such as gypsum, while no evaporite was found in the study area. If SO_4^{2-} comes from the gypsum dissolution, the ratios of Ca^{2+} and SO_4^{2-} should be close to 1:1. The stoichiometric analysis (Fig.2) showed that the ratio of Ca^{2+} and SO_4^{2-} deviated from 1:1 and also proved this point.

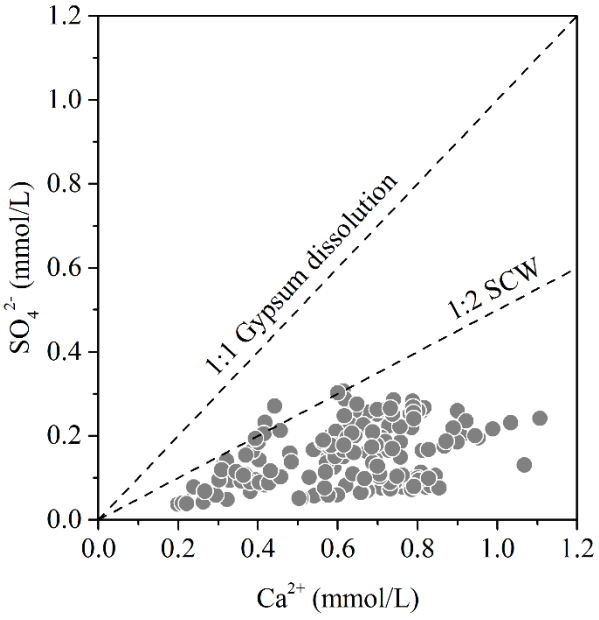

Fig. 2 Stoichiometric relationship between Ca^{2+} and SO_4^{2-}. The "SCW" means carbonate weathering induced by sulfuric acid

So that, on the basis of the theory of rock chemical weathering and ignoring the anthropogenic origins of major ions (except for SO_4^{2-}), the major elements of river water can be simplified as

followed:

$$[Cl^-]_{riv} = [Cl^-]_{pre} + [Cl^-]_{eva} \quad (2)$$

$$[K^+]_{riv} = [K^+]_{pre} + [K^+]_{sil} \quad (3)$$

$$[Na^+]_{riv} = [Na^+]_{pre} + [Na^+]_{eva} + [Na^+]_{sil} \quad (4)$$

$$[Ca^{2+}]_{riv} = [Ca^{2+}]_{pre} + [Ca^{2+}]_{sil} + [Ca^{2+}]_{car} \quad (5)$$

$$[Mg^{2+}]_{riv} = [Mg^{2+}]_{pre} + [Mg^{2+}]_{sil} + [Mg^{2+}]_{car} \quad (6)$$

$$[HCO_3^-]_{sil} = [K^+]_{sil} + [Na^+]_{sil} + 2[Mg^{2+}]_{sil} + 2[Ca^{2+}]_{sil} \quad (7)$$

$$[HCO_3^-]_{car} = [HCO_3^-]_{riv} - [HCO_3^-]_{sil} \quad (8)$$

$$[SO_4^{2-}]_{riv} = [SO_4^{2-}]_{pre} + [SO_4^{2-}]_{anth} \quad (9)$$

Firstly, the measured ion concentrations of the rain water are rectified by evaporation coefficient α=0.63=P/R (with P the precipitation and R the runoff) and calculated the contributions of atmospheric precipitation. Secondly, the molar ratios of Ca^{2+}/Na^+ (0.4) and Mg^{2+}/Na^+ (0.2) for silicate end-member (Zhang et al., 2007) are used to calculate the contribution of Ca^{2+} and Mg^{2+} from silicate weathering, and then, residual Ca^{2+} and Mg^{2+} were attributed to carbonate weathering. For monthly data, the contributions of different sources can be calculated as followed:

$$R_{car}=([Ca^{2+}]_{car}+[Mg^{2+}]_{car})/S \times 100\% \quad (10)$$

$$R_{sil}=([K^+]_{sil}+[Na^+]_{sil}+[Ca^{2+}]_{sil}+[Mg^{2+}]_{sil})/S \times 100\% \quad (11)$$

$$R_{eva}=[Na^+]_{eva}/S \times 100\% \quad (12)$$

$$R_{pre}=([K^+]_{pre}+[Na^+]_{pre}+[Ca^{2+}]_{pre}+[Mg^{2+}]_{pre})/S \times 100\% \quad (13)$$

$$S = [Ca^{2+}]_{car} + [Mg^{2+}]_{car} + [Ca^{2+}]_{sil} + [Mg^{2+}]_{sil} + [Na^+]_{sil} + [K^+]_{sil} + [Na^+]_{eva} + [Ca^{2+}]_{pre} + [Mg^{2+}]_{pre} + [Na^+]_{pre} + [K^+]_{pre} \quad (14)$$

Where *R* denotes the proportions of dissolved cations from different sources. *S* denotes the total

178 concentrations of cations for river water in mmol·L^{-1}.

179 The total, carbonate and silicate chemical weathering rates (TWR, CWR and SWR) of a year

180 can be estimated as followed:

181 $$CWR=\sum_{i=1}^{n=12}[\left(24\times\left[Mg^{2+}\right]_{car}+40\times\left[Ca^{2+}\right]_{car}+61\times[HCO_3^-]_{car}\times 0.5\right)_i\times Q_i/(10^6A)] \quad (15)$$

182 $$SWR=\sum_{i=1}^{n=12}[\left(39\times\left[K^+\right]_{sil}+23\times\left[Na^+\right]_{sil}+24\times\left[Mg^{2+}\right]_{sil}+40\times\left[Ca^{2+}\right]_{sil}+96\times[SiO_2]_{sil}\right)_i\times$$

183 $$Q_i/(10^6A)] \quad (16)$$

184 $$TWR=CWR+SWR \quad (17)$$

185 Where TWR, CWR and SWR have the unit of t km^{-2} a^{-1}, Q_i denotes discharge in m^3·$month^{-1}$, and A

186 denotes the catchment area in km^2.

187 **3.2.2 DIC apportionments**

188 In the Beijiang River, the pH values of water samples ranged from 7.5 to 8.5 with an average

189 of 8.05. Under this pH conditions, the major species of DIC is HCO_3^-. In addition, HCO_3^- accounted

190 for more than 95% in all sampling sites based on calculation, thus the concentration of HCO_3^-

191 (mmol/L) was used to represent the DIC concentration in this study. The riverine DIC originates

192 from several sources including carbonate minerals, respired soil CO_2 and atmospheric CO_2, and it

193 could be affected by processes occurring along the water pathways (Khadka et al., 2014; Li et al.,

194 2008). Four dominant weathering processes, including (1) carbonate weathering by carbonic acid

195 (CCW), (2) carbonate weathering by sulfuric acid (SCW), (3) silicate weathering by carbonic acid

196 (CSW), (4) and silicate weathering by sulfuric acid (SSW), can be described by the following

197 reaction equations:

198 $$CCW:(Ca_{2-x}Mg_x)(CO_3)_2+2H_2CO_3\rightarrow(2-x)Ca^{2+}+xMg^{2+}+4HCO_3^- \quad (18)$$

199 $$SCW:(Ca_{2-x}Mg_x)(CO_3)_2+H_2SO_4\rightarrow(2-x)Ca^{2+}+xMg^{2+}+2HCO_3^-+SO_4^{2-} \quad (19)$$

200 $$\text{CSW:}CaSiO_3 + 2H_2CO_3 + H_2O \rightarrow Ca^{2+} + H_4SiO_4 + 2HCO_3^- \quad (20)$$

201 $$\text{SSW:}CaSiO_3 + H_2SO_4 + H_2O \rightarrow Ca^{2+} + H_4SiO_4 + SO_4^{2-} \quad (21)$$

202 Where $CaSiO_3$ represents an arbitrary silicate.

203 According to the study of Galy and France-Lanord (1999) and Spence and Telmer (2005),
204 carbonate and silicate weathering by carbonic acid in the same ratio as carbonate and silicate
205 weathering by sulfuric acid, for monthly data the mass balance equations are followed:

206 $$[SO_4^{2-}]_{riv} - [SO_4^{2-}]_{pre} = [SO_4^{2-}]_{SCW} + [SO_4^{2-}]_{SSW} \quad (22)$$

207 $$[SO_4^{2-}]_{riv} - [SO_4^{2-}]_{pre} = \alpha_{SCW} \times [HCO_3^-]_{riv} \times 0.5 + \frac{\alpha_{CSW} \times \alpha_{SCW}}{\alpha_{CCW}} \times [HCO_3^-]_{riv} \quad (23)$$

208 Where the subscripts CCW, SCW, CSW and SSW denotes the four end-members defined by
209 carbonate weathering by carbonic acid, carbonate weathering by sulfuric acid, silicate weathering
210 by carbonic acid and silicate weathering by sulfuric acid, respectively. The parameter α denotes the
211 proportion of DIC derived from each end-member processes.

212 According to the above description, the ion balance equations are followed:

213 $$[Ca^{2+}]_{car} + [Mg^{2+}]_{car} = \alpha_{CCW} \times [HCO_3^-]_{riv} \times 0.5 + \alpha_{SCW} \times [HCO_3^-]_{riv} \quad (24)$$

214 $$[SO_4^{2-}]_{SCW} + [SO_4^{2-}]_{SSW} = \alpha_{SCW} \times [HCO_3^-]_{riv} \times 0.5 + \frac{\alpha_{CSW} \times \alpha_{SCW}}{\alpha_{CCW}} \times [HCO_3^-]_{riv} \quad (25)$$

215 $$\alpha_{CCW} + \alpha_{SCW} + \alpha_{CSW} = 1 \quad (26)$$

216 Combing the above equations, the proportions of HCO_3^- derived from three end-members
217 (CCW, SCW and CSW) can be calculated, and the DIC (equivalent to HCO_3^-) fluxes by different
218 chemical weathering processes are calculated by following equations.

219 $$[HCO_3^-]_{CCW} = \alpha_{CCW} \times [HCO_3^-]_{riv} \quad (27)$$

220 $$[HCO_3^-]_{SCW} = \alpha_{SCW} \times [HCO_3^-]_{riv} \quad (28)$$

221 $$[HCO_3^-]_{CSW} = \alpha_{CSW} \times [HCO_3^-]_{riv} \quad (29)$$

3.2.3 CO_2 consumption rate and CO_2 net sink

According to the equations (17)~(20), only the processes of CCW and CSW can consume the CO_2 from atmosphere or soil and only half of the HCO_3^- in the water due to carbonate weathering by carbonic acid come from atmospheric CO_2. Thus, the CO_2 consumption rates (CCR) for CCW and CSW can be calculated as followed (Zeng et al., 2016):

$$\mathrm{CCR_{CCW}} = \sum_{i=1}^{n=12}\{[0.5 \times (\mathrm{Q/A}) \times [\mathrm{HCO_3^-}]_{\mathrm{CCW}}]/1000\}_i \quad (30)$$

$$\mathrm{CCR_{CSW}} = \sum_{i=1}^{n=12}\{[(\mathrm{Q/A}) \times [\mathrm{HCO_3^-}]_{\mathrm{CSW}}]/1000\}_i \quad (31)$$

Where Q is discharge in $m^3 \cdot a^{-1}$, $[HCO_3^-]$ is concentration of HCO_3^- in $mmol \cdot L^{-1}$, A is catchment area in km^2, so that the CCR has the unit of 10^3 mol $km^{-2} \cdot a^{-1}$.

According to the classical view of the global carbon cycling (Berner and Kothavala, 2001), the CCW is not a mechanism that can participate to the amount of CO_2 in the atmosphere because all of the atmospheric fixed through CCW is returned to the atmosphere during carbonate precipitation in the ocean. However, when sulfuric acid is involved as a proton donor in carbonate weathering, half of the dissolved carbon re-release to the atmospheric during carbonate precipitation. Thus, SCW leads to a net release of CO_2 in ocean-atmosphere system over timescale typical of residence time of HCO_3^- in the ocean (10^5 years). Meanwhile, in case of CSW, followed by carbonate deposition, one of the two moles of CO_2 involved is transferred from the atmosphere to the lithosphere in the form of carbonate rocks, while the other one returns to the atmosphere, resulting a net sink of CO_2. Therefore, the net CO_2 consumption rate (CCR_{Net}) due to chemical weathering can be concluded as followed:

$$\mathrm{CCR_{Net}} = \sum_{i=1}^{n=12}\{[(0.5 \times [\mathrm{HCO_3^-}]_{\mathrm{CSW}} - 0.5 \times [\mathrm{HCO_3^-}]_{\mathrm{SCW}}) \times (\mathrm{Q/A})]/1000\}_i \quad (32)$$

3.3 Spatial and statistical analysis

The hypsometric integral value (HI) (PIKE and WILSON, 1971) was employed in this study to evaluate the influence of terrain on the chemical weathering. HI is an important index to reveal the relationship between morphology and development of landforms and can be used to establish the quantitative relationship between the stage of geomorphological development and the material migration in the basin (PIKE and WILSON, 1971; Singh et al., 2008; STRAHLER, 1952). The HI value of each watershed is calculated by the elevation-relief ratio method and can be obtained by the following equation (PIKE and WILSON, 1971):

$$HI = \frac{\text{Mean.elevation} - \text{Min.elevation}}{\text{Max.elevation} - \text{Min.elevation}} \quad (33)$$

Where HI is the hypsometric integral; Mean.elevation is the mean elevation of the watershed; Min.elevation is the minimum elevation within the watershed; Max.elevation is the maximum elevation within the watershed. According to the hypsometric integral value (HI), the geomorphological development can be divided into three stages: inequilibrium or young stage ($HI > 0.6$), equilibrium or mature stage ($0.35 < HI \leqslant 0.6$), and monadnock or old age ($HI \leqslant 0.35$), which can reflect the erodible degree and erosion trend of the geomorphology (Xiong et al., 2014).

The watershed of the study area was divided by using hydrological analysis module of ArcGIS. The average slope and HI was conducted by spatial analysis module of ArcGIS. The area of silicate/carbonate outcrops was calculated by hydrological module of ArcGIS based on geology map from provided by China Geological Survey. The data of river water discharge was provided by the local hydrology bureau.

All statistical tests were conducted using SPSS version 22.0. One-way analysis of variance (ANOVA) was performed to check the differences of monthly major ion concentrations and

dissolved inorganic carbonate isotopes with significance at $p<0.05$. Principal component analysis (PCA) was employed to unravel the underlying data set through the reduced new variables, analyzed the significant factors affecting the characteristics of water chemistry.

4 Results

4.1 Chemical compositions

The major physical-chemical parameters of river water samples were presented in Table 1. In Table 1, the chemical parameters of river water were the flow-weighted average over 12 months. For every sampling station, the flow-weighted average of ion concentration can be expressed followed the equation $[X]_{avarage} = \frac{\sum_{i=1}^{n=12}[X]_i \times Q_i}{\sum_{i=1}^{n=12} Q_i}$, where [$X$] denotes the elements of Ca^{2+}, Mg^{2+}, Na^{+}, K^{+}, Cl^{-}, SO_4^{2-}, HCO_3^{-} in $mmol \cdot L^{-1}$. Q denotes average monthly discharge in $m^3\ s^{-1}$. The subscripts i denotes 12 months from January to December. For all the monthly samples, the pH values ranged from 7.5 to 8.5 with an average of 8.05. Average EC was 213 $\mu s \cdot cm^{-1}$, ranging from 81 to 330 $\mu s \cdot cm^{-1}$. The TDS of river water samples varied from 73.8 to 230.2 $mg \cdot L^{-1}$, with an average of 157.3 $mg \cdot L^{-1}$, which was comparable with the global average of 100 $mg \cdot L^{-1}$ (Gaillardet et al., 1999). Compared with the major rivers in China, the average TDS was significantly lower than the Changjiang (Chen et al., 2002) , the Huanghe (He Jiangyi, 2017) the Zhujiang (Zhang et al., 2007), the Huaihe (Zhang et al., 2011) and the Liaohe (Ding et al., 2017). However, the average TDS was higher than the rivers draining silicate-rock-dominated areas, e.g., Dojiang River (59.9 $mg \cdot L^{-1}$) in Southern China (Xie Chenji, 2013), North Han River (75.5 $mg \cdot L^{-1}$) in South Korea, (Ryu et al., 2008), the Amazon (41 $mg \cdot L^{-1}$) and the Orinoco (82 $mg \cdot L^{-1}$) draining the Andes (Dosseto et al., 2006; Edmond et al., 1996).

Table 1 The major physical-chemical parameters of river water samples at 15 hydrological station in the Beijiang River (mean±SD). The total dissolved solid (TDS, mg·L^{-1}) expressed as the sum of major inorganic species concentration (Na^++K^++Ca^{2+}+Mg^{2+}+HCO_3^-+Cl^-+SO_4^{2-}+NO_3^-+SiO_2)

Hydrological stations	pH	EC (μs/cm)	TDS (mg/L)	Na^+ (μmol/L)	K^+ (μmol/L)	Ca^{2+} (μmol/L)	Mg^{2+} (μmol/L)	HCO_3^- (μmol/L)	Cl^- (μmol/L)	SO_4^{2-} (μmol/L)	SiO_2 (μmol/L)	HI
JLWs	7.9±0.2	95±40	81.1±25.6	111.4	51.9	223.5	103.9	701.9	28.3	44.5	225.2	0.34
CXs	8.2±0.2	219±50	163.7±20.9	118.1	40.1	793.3	187.1	1593.6	60.5	199.4	106.3	0.29
HJTs	8.1±0.2	203±34	151.8±21.9	100.2	29.9	686.7	203.9	1708.7	29.5	72.2	156.6	0.30
ZKs	8.1±0.1	218±45	161.3±21.1	426.4	66.2	560.3	134.1	1276.9	134.7	161.4	151.9	0.22
XGLs	7.8±0.2	168±16	117.9±8.9	315.4	112.4	422.4	101.0	992.2	213.9	112.6	178.9	0.18
WJs	8.1±0.1	260±27	172.9±16.7	197.8	59.0	767.3	122.6	1467.1	99.1	162.8	183.4	0.25
LXs	8.1±0.2	236±33	171.8±19.6	122.1	38.1	813.5	176.0	1829.4	51.5	89.2	145.7	0.21
LCs	8.2±0.1	253±26	196.1±20.0	287.4	46.8	862.6	234.4	1845.7	115.7	232.4	130.7	0.27
LSs	8.3±0.1	220±46	184.2±18.3	258.9	58.2	793.5	202.9	1740.6	109.0	191.9	121.4	0.25
XSs	7.9±0.1	156±30	123.9±17.6	305.0	86.1	366.8	110.9	966.6	103.8	166.5	218.7	0.24
GDs	8.1±0.1	232±11	169.4±8.3	112.6	40.5	781.6	172.1	1798.5	44.0	90.3	141.2	0.24
SKs	8.1±0.2	238±22	161.1±17.4	345.3	73.6	641.0	162.5	1304.1	174.4	223.5	160.1	0.21
Yds	7.8±0.2	241±54	165.9±34.0	296.4	59.3	674.8	160.9	1515.0	118.7	175.9	144.4	0.21
FLXs	8.0±0.2	232±37	161.4±22.8	187.6	95.1	577.0	135.0	1262.4	111.9	159.6	169.5	0.21
SJs	8.1±0.1	230±27	176.4±18.9	355.0	83.4	663.5	156.2	1367.7	182.4	190.5	180.5	0.21

Major ion compositions were shown in the Piper plot (Fig. 3). Ca^{2+} was the dominant cation with concentration ranging from 199 to 1107 μmol·L^{-1}, accounting for approximately 49% to 81%, with an average of 66% (in μEq) of the total cation composition in the river water samples. HCO_3^- was the dominant anion, with concentration ranging from 640 to 2289 μmol·L^{-1}. On average, it comprised 77% (59%~92%) of total anions, followed by SO_4^{2-} (16%) and Cl^- (6%). The major ionic composition indicated that the water chemistry of the Beijiang River Basin was controlled by both carbonate and silicate weathering.

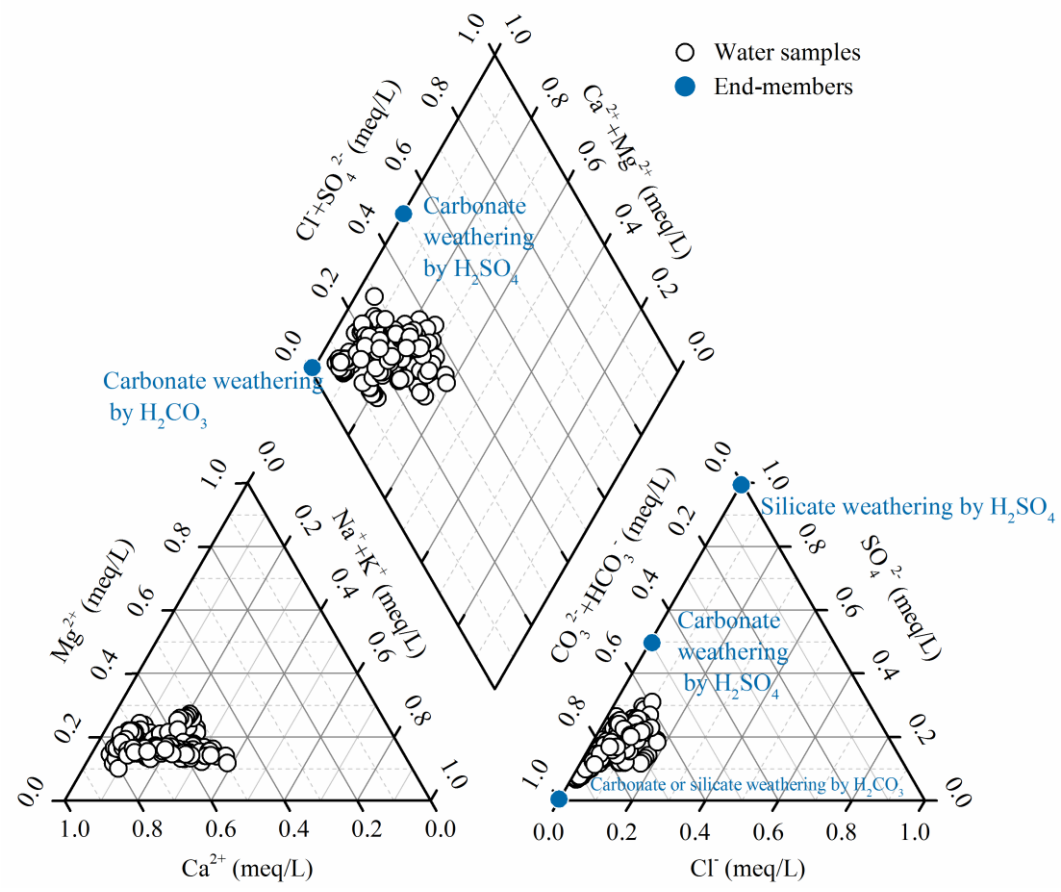

Fig. 3 Piper plot of river water samples in the Beijiang River

The PCA was used to extract the factors controlling the chemical compositions. The varimax rotation was used to reduce the number of variables to two principal components (PCs), which together explain 76.88% of the total variance in the data. The first PC (PC1) explained

301 approximately 50.02% of the total variations, and was considered to represent "carbonate
302 weathering factor" because of the high loadings of EC, TDS, Ca^{2+}, Mg^{2+} and HCO_3^- concentrations.
303 The second PC (PC2) explained 26.85% of the total variance and presented high loadings for Na^+
304 and K^+ concentrations. Thus, the PC2 represented a "silicate weathering factor". These two PCs
305 were considered to be two important sources of major ions in the Beijiang River Basin.

306 The hydrochemical compositions of rain water were presented in Table S1. Ca^{2+} was the
307 dominant cation with concentration ranging from 6.9 to 282.6 μmol·L^{-1}, accounting for
308 approximately 65% of the total cation composition in the rain water samples. SO_4^{2-} was the
309 dominant anion, with concentration ranging from 21.9 to 1462 μmol·L^{-1}, accounting for
310 approximately 67% of the total anion composition in the rain water samples.

311 **4.2 Seasonal and spatial variations**

312 There were significant seasonal variations in the major ion concentrations (Fig. 4). Two basic
313 patterns of temporal variations could be observed. The first one was related to the carbonate
314 weathering derived ions such as Ca^{2+} and HCO_3^-, which showed high values in November and low
315 values in June. The second one was for the silicate weathering derived ions such as Na^+ and K^+,
316 which showed high values in February and low values in June. The minimums occurred in Jun for
317 all the ions showed a significant dilution effect during the high-flow periods.

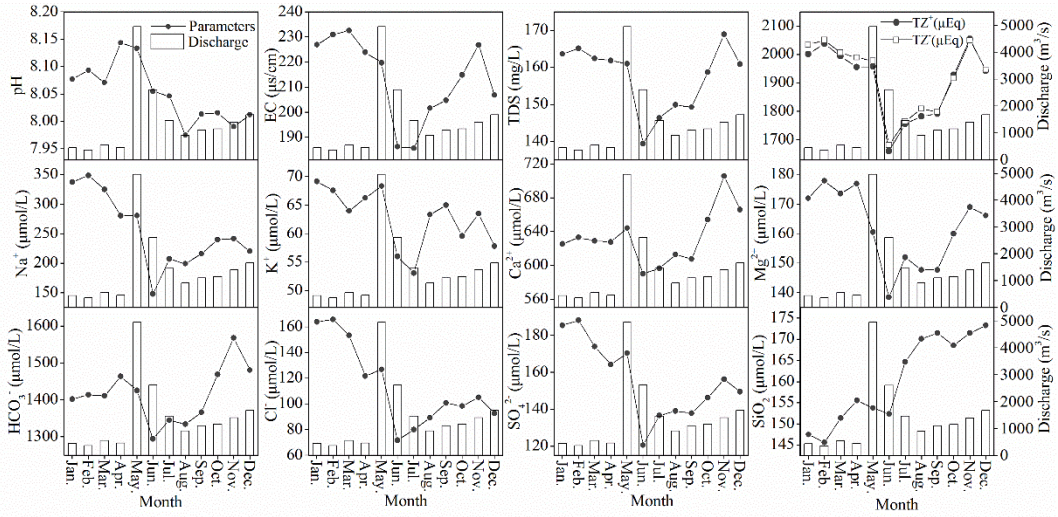

Fig. 4 Monthly variations of environmental parameters and major ion concentrations in the Beijiang River Basin (SJs station). The columns denoted the monthly discharge

It was clear that the Ca^{2+} and HCO_3^- concentrations had a decreasing trend from upstream to downstream (Fig. 5), this characteristic agrees with the trends observed in the Changjiang River and the Huai River, where the major elements or TDS concentrations of the main channel showed a general decreasing trend, and the tributaries display the dilution effect to the main channel. For other silicate weathering derived ions such as Na^+, there was a slight increasing trend implying the chemical inputs from the tributaries. These trends were in accordance with the lithology in the study area. The carbonate is dominated in the upper stream basin, when river drainages this area, carbonate weathering contributes to the elevation of Ca^{2+} and HCO_3^-. As the river entered into the downstream dominated with silicate, the relative low ion concentrations due to silicate weathering contributed to diluting the Ca^{2+} and introducing extra Na^+ to the main channel.

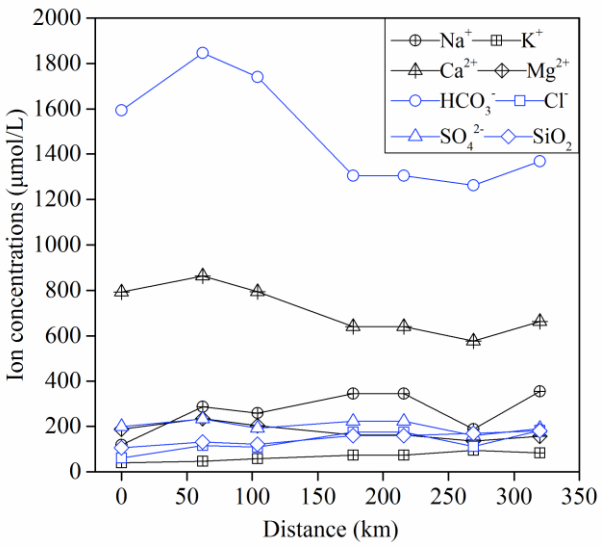

Fig. 5 Spatial variations of major ion and SiO2 concentrations in the Beijiang River Basin (From upstream station CXs to the downstream station SJs)

5 Discussion

5.1 Chemical weathering rates and the controlling factors

5.1.1 Chemical weathering rates

Atmospheric precipitation inputs, anthropogenic inputs (here refer to the acid depostion and AMD) and chemical weathering of rocks and minerals as the major sources contributed to the hydrochemistry in the river basin. Previous studies have shown that rock weathering contributions to major element composition of the river can be interpreted in terms of mixing among three main end-members: the weathering products of carbonates, silicates and evaporites (Cao et al., 2016b; Négrel et al., 1993; Ollivier et al., 2010). The river water samples in the Beijiang River Basin were displayed on the plots of Na-normalized molar ratios (Fig. 6). In these plots, the contributions from carbonate weathering correspond to the trend toward high-Ca^{2+} end-member close to the top right corner, while silicate weathering correspond to the trend toward to high-Na^{+} end-member close to the low-left corner. It was clear that the samples with high ratio of carbonate outcrop had the highest molar ratios of Ca^{2+}/Na^{+}, Mg^{2+}/Na^{+} and HCO_3^{-}/Na^{+}, which made the samples located toward to the

carbonate weathering end-member. However, the samples with low Ca^{2+}/Na^{+}, Mg^{2+}/Na^{+} and HCO_3^{-}/Na^{+} ratios showed the influence of silicate weathering. In addition, major ion compositions of the Beijiang River were mainly contributed by the weathering of carbonates and silicates, and showed little contribution of evaporite weathering.

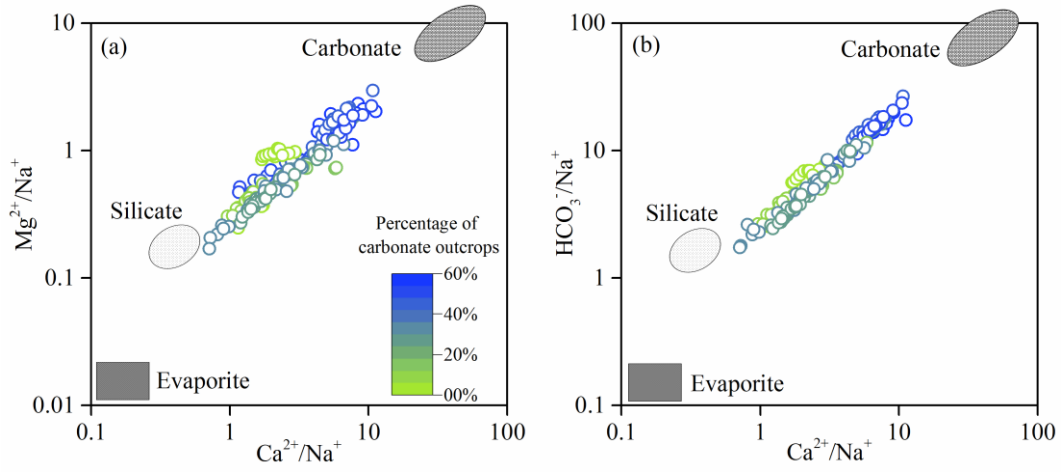

Fig. 6 Mixing diagrams using Na-normalized molar ratios: (a) Mg^{2+}/Na^{+} vs. Ca^{2+}/Na^{+} (b) HCO_3^{-}/Na^{+} vs. Ca^{2+}/Na^{+} for the Beijiang River Basin. The color ramp showed the percentage of carbonate outcrops

Based on the chemical balance method, the calculated contributions of different sources to the total cationic loads were presented in Fig. 7. The results showed that carbonate weathering was the most important mechanism controlling the local hydrochemistry, and contributed approximately 50.06% (10.96%~79.96%) of the total cationic loads. Silicate weathering and atmospheric precipitation inputs accounted for 25.71% (5.55%~70.38%) and 17.92% (0~46.95%), respectively. Evaporite weathering had the minimum contribution with an average of 6.31% (0~24.36%) to the total cationic loads.

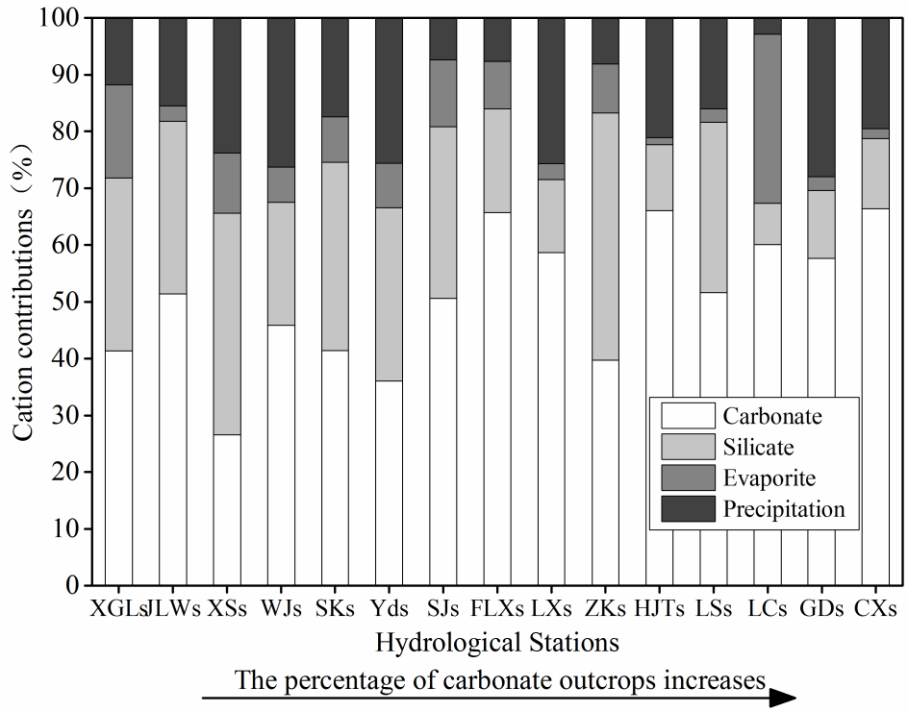

363

364 **Fig. 7 Calculate contributions (in %) from the different hydrological stations to the total cationic**

365 **load in the Beijiang River Basin. The cationic loads were the sum of Na^+, K^+, Ca^{2+} and Mg^{2+}**

366 The result of chemical weathering rates was listed in Table 2. The carbonate weathering

367 contributes about 70% of the total chemical weathering, and the average of carbonate and silicate

368 weathering rate in the Beijiang River Basin were 61.15 and 25.31 $t \cdot km^{-2} \cdot a^{-1}$, respectively. In addition,

369 chemical weathering rates showed significantly seasonal variations with the highest carbonate and

370 silicate weathering rates in May (16.75 and 5.50 $t \cdot km^{-2} \cdot month^{-1}$, respectively) and the lowest

371 carbonate and silicate weathering rates in February (0.95 and 0.39 $t \cdot km^{-2} \cdot month^{-1}$, respectively).

372 Gaillardet et al. (1999) reported the chemical weathering rate of major rivers all over the world and

373 found that the hyperactive zone with high chemical weathering rate is generally located between the

374 latitude 0-30^o and our study belongs to this area (Fig. 8). The factors influence the balance between

375 CWR and SWR would be further discussed in the following parts.

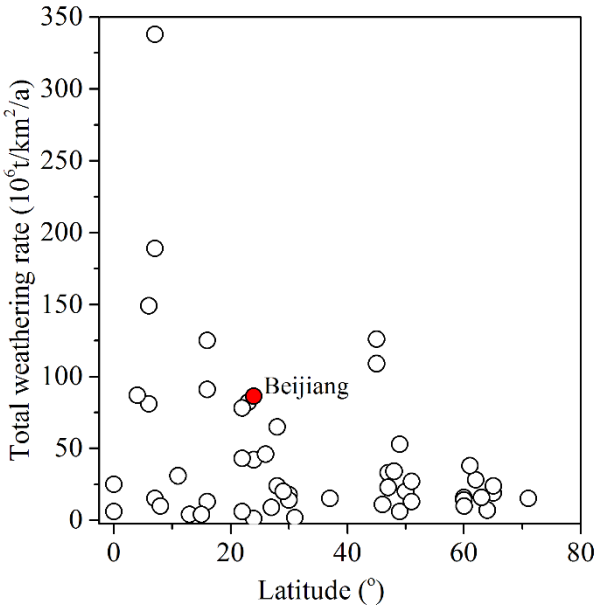

376

377 **Fig. 8 Relationship between latitude and total weathering rate (TWR)**

378 **Table 2 The annual discharge, catchment area, carbonate and silicate outcrops proportions, and**

379 **calculated weathering rates of carbonate and silicate of 15 subcatchments in the Beijiang River**

ID	Annual discharge (10^8m^3/a)	Catchment area (km^2)	Percentages of carbonate (%)	Percentages of silicate (%)	Carbonate weathering rate -CWR (t km^{-2} year^{-1})	Silicate weathering rate -SWR (t km^{-2} year^{-1})	Total weathering rate -TWR (t km^{-2} year^{-1})
JLWs	2.23	281.13	2.95	97.05	18.63	14.94	33.56
CXs	4.06	392.35	57.44	42.56	74.21	11.42	85.64
HJTs	11.54	503.02	41.99	55.83	169.12	29.73	198.85
ZKs	16.38	1655.22	34.60	61.81	35.03	24.14	59.17
XGLs	13.56	1863.02	0.38	93.07	25.75	13.96	39.72
WJs	19.11	1960.99	12.51	73.87	55.00	17.43	72.43
LXs	56.37	2458.06	34.32	64.07	178.71	29.39	208.10
LCs	58.74	5278.14	49.67	50.21	79.70	20.59	100.29
LSs	74.83	6994.69	44.59	52.44	69.28	14.94	84.22
XSs	62.11	7497.01	7.09	87.81	18.85	20.35	39.20
GDs	137.81	9028.38	49.93	44.93	111.73	19.19	130.92
SKs	49.51	17417.24	25.43	69.35	12.71	6.11	18.82
YDs	191.07	18234.64	25.63	68.05	52.37	19.59	71.95
FLXs	396.25	34232.34	29.68	63.49	68.38	17.53	85.91
SJs(Average)	450.90	38538.06	28.12	64.65	61.15	25.31	86.46

380 **5.1.2 Factors affecting chemical weathering**

381 Many factors control the chemical weathering rates, including terrain, geotectonic properties,

382 lithology, land cover, climatic conditions (temperature, precipitation, etc.), and hydrological
383 characteristics (Ding et al., 2017; Gislason et al., 2009; Hagedorn and Cartwright, 2009). For this
384 study, the lithology, hydrological characteristics and geomorphology was selected as the major
385 factors to be discussed.

386 **5.1.2.1 Lithology**

387 Among all the factors controlling the chemical weathering rates, lithology is one of the most
388 important factors because different type of rocks has different weathering abilities (Viers et al.,
389 2014). The TWR had a significant positive correlation (p<0.01) with the ratios of the proportion of
390 carbonate and a non-significant positive correlation with that of silicate outcrops (Fig. 9a, b).
391 Furthermore, a significant correlation (p<0.01) was found between the CWR and proportion of
392 carbonate outcrops (Fig. 9c), but the correlation between the SWR and the proportion of silicate
393 outcrops was low and not statistically significant (p>0.05, Fig. 9d). The correlation analysis
394 confirmed that carbonate outcrops ratios was the sensitive factor controlling the chemical
395 weathering rates and the rapid kinetics of carbonate dissolution played an important role in
396 weathering rates in the Beijiang River Basin.

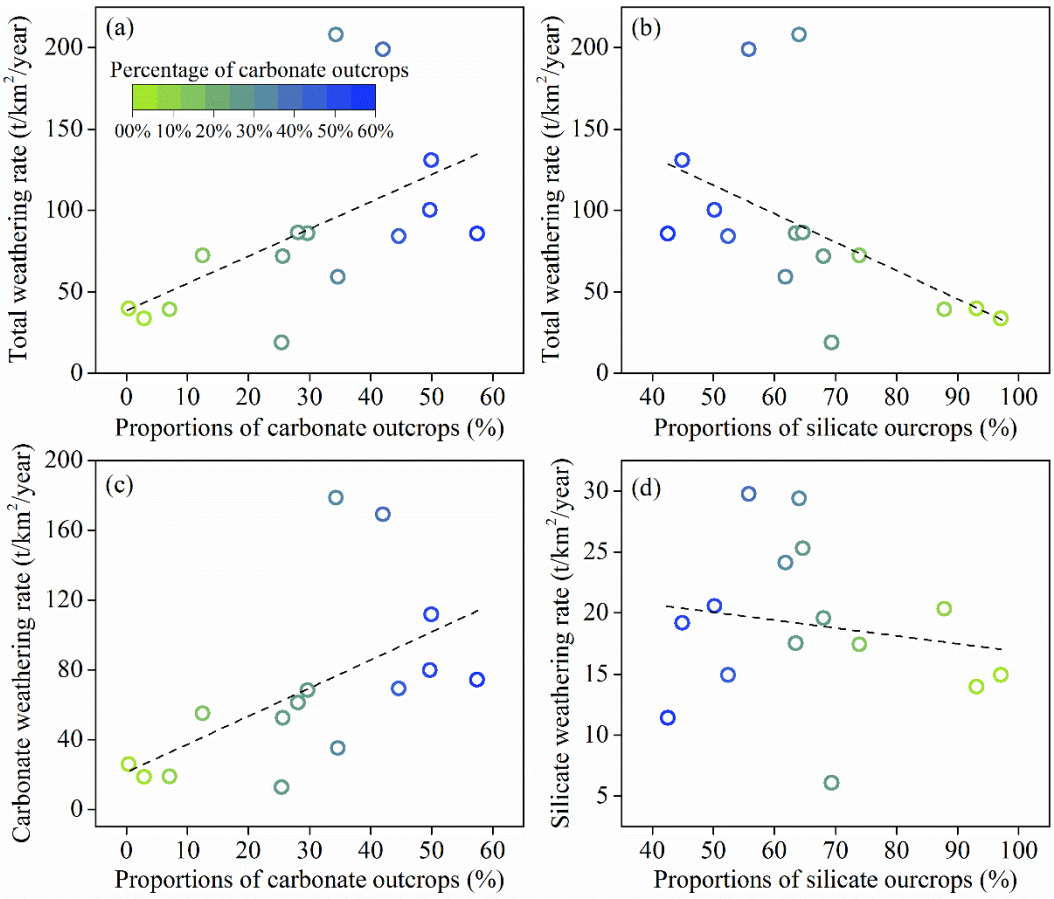

Fig. 9 The relationships between weathering rates and the proportions of carbonate or silicate outcrops

5.1.2.2 Runoff

Chemical weathering is a combination of two processes, including dissolution of primary minerals and precipitation of secondary minerals growth (Eiriksdottir et al., 2011; Hartmann et al., 2014a; Liu et al., 2013). The dissolution process is quite related to the precipitation and runoff. In general, river water chemistry is usually diluted by river runoff (Q), and this dilution effect is variable in different basins (Rao et al., 2019). The dilution effects of major element caused by increasing water flow can be expressed by log linear equation, the standard rating relationship (Li et al., 2014; Walling, 1986; Zhang et al., 2007):

$$C_i = aQ^b \quad (34)$$

where C_i is the concentration of element i (mmol/L), Q is the water discharge (m^3/s), a is the regression constant and b is the regression exponent. The linear fitting result was showed by Fig. 10 and the parameters b for major elements obtained from the dataset were 0.08 (Na^+), 0.05 (K^+), 0.08 (Ca^{2+}), 0.02 (Mg^{2+}), 0.06 (HCO_3^-), 0.12 (Cl^-), 0.11 (SO_4^{2-}) and -0.005 (SiO_2), respectively. In many cases, b ranges from -1 to 0 due to the chemical variables that are influenced in various ways and various extents. However, in our study area, the values of b were positive and not comparable to the observations in the major Asian River such as the Yangtze (Chen et al., 2002), the Yellow (Chen et al., 2005), the Pearl Rivers (Zhang et al., 2007) and the Mekong River (Li et al., 2014). This suggested additional and significant solute sources in the river basin that might contribute and compensate considerably the effect of dilution by precipitation. The difference of slope for individual dissolved components at different stations reflected the different sources and the solubility of source materials.

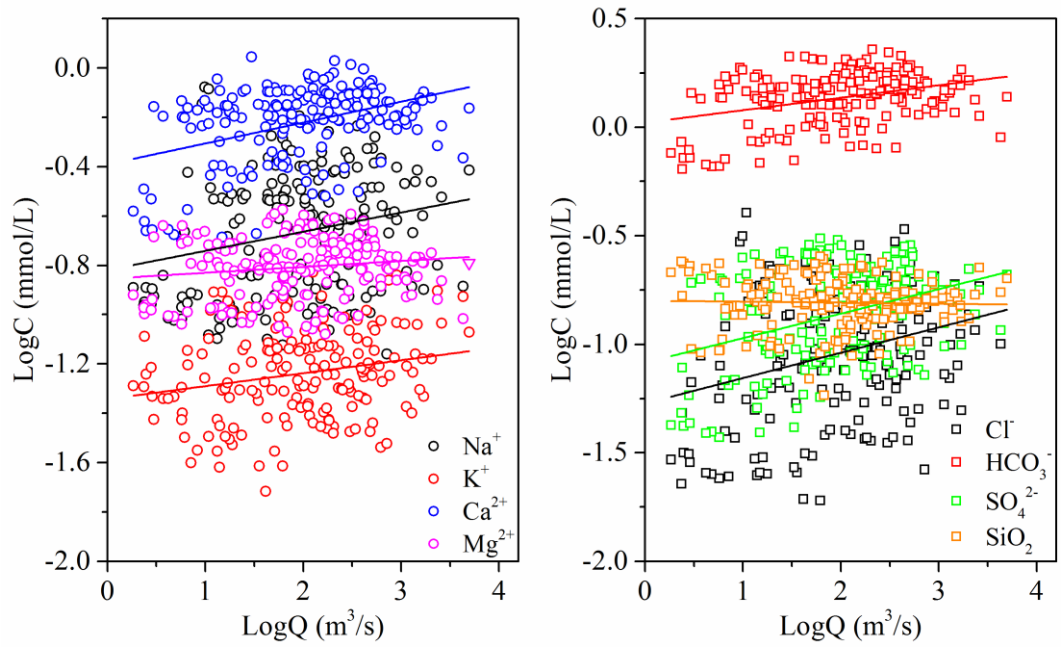

Fig. 10 The relationship between major ion concentrations and runoff (Q) in logarithmic scales

Due to the compensation effect of chemical weathering, significant positive linear relationship

was detected between Q and TWR, CWR and SWR. So that, the linear regression analysis between Q and TWR, CWR and SWR were conducted to further reveal the effect of runoff on chemical weathering rate. The slope of the liner regression equations for all 15 hydrological station watersheds in the Beijiang River Basin were summarized in Table 3. The linear relations indicated that the increase of runoff could accelerate the chemical weathering rates, but the variations of K values revealed that the degrees of influences were different due to multiple factor influence, such as the influence of geomorphology.

Table 3 The slope of the liner regression equation between runoff (Q) and total weathering rate (TWR), carbonate weathering rate (CWR) and silicate weathering rate (SWR)

Hydrological stations	Total weathering rate $=K_1Q$		Carbonate weathering rate $=K_2Q$		Silicate weathering rate $=K_3Q$	
	K_1	R^2	K_2	R^2	K_3	R^2
JLWs	0.3912	0.99	0.2091	0.99	0.1821	0.99
CXs	0.6492	0.93	0.5631	0.93	0.0860	0.94
HJTs	0.5117	0.97	0.4421	0.96	0.0695	0.99
ZKs	0.0953	0.97	0.0525	0.76	0.0429	0.80
XGLs	0.0835	0.98	0.0558	0.97	0.0278	0.98
WJs	0.1017	0.99	0.0842	0.99	0.0175	0.88
LXs	0.0968	0.98	0.0843	0.98	0.0125	0.99
LCs	0.0486	0.90	0.0401	0.87	0.0085	0.97
LSs	0.0359	0.97	0.0286	0.96	0.0073	0.94
XSs	0.0180	0.98	0.0080	0.97	0.0100	0.96
GDs	0.0252	0.99	0.0216	0.99	0.0036	0.99
SKs	0.0116	0.98	0.0083	0.98	0.0033	0.95
Yds	0.0106	0.99	0.0081	0.99	0.0026	0.92
FLXs	0.0050	0.97	0.0039	0.95	0.0010	0.99
SJs	0.0053	0.99	0.0037	0.97	0.0016	0.98

5.1.2.3 Geomorphology

The geomorphology factors including catchment area, average slope and HI, which could quite

435 influence the runoff generation process and physical and chemical weathering, were selected to give
436 a further explanation of the variation of K values. As showed in Fig. 11a, the K values were found
437 a non-linear relationship with the areas of subcatchment and could be fitted by exponential decay
438 model, which showed that the K values decreased dramatically with the initial increasing of area
439 and quickly become stable after reaching the threshold. The threshold value for K_1, K_2 and K_3 was
440 about 5000 km^2. It indicated that the compensation effect was more significant in small catchment.
441 The average topographic slope of each subcatchment ranged from 37^o to 63^o. With the
442 increasing of average slope, the residence time of both surface water and groundwater decrease.
443 Kinetics of carbonate and silicate reactions was determined by the reaction time which could be
444 related by the residence time of water. In our study area, the K values showed non-linear negative
445 correlation with average slope (Fig. 11e, f, g). When the average slope increase, the resulted small
446 residence time (time of water-rock reactions) make the compensation effect also weak in the study
447 area.
448 Hypsometric analysis showed that the HI ranged from 0.18 to 0.34. According to the empirical
449 classification by HI ($HI > 0.6$, inequilibrium or young stage, $0.35 < HI \leq 0.6$, equilibrium or mature
450 stage, $HI \leq 0.35$, monadnock or old age), the geomorphological development in the Beijiang River
451 was recognized as the old age, which reflect the erodible degree and erosion trend of the
452 geomorphology was high. Furthermore, the non-linear positive correlations between HI and K
453 values (Fig. 11g, h, i) also addressed that geomorphology development have significant influence
454 on chemical weathering and relating CO_2 consumption processes.

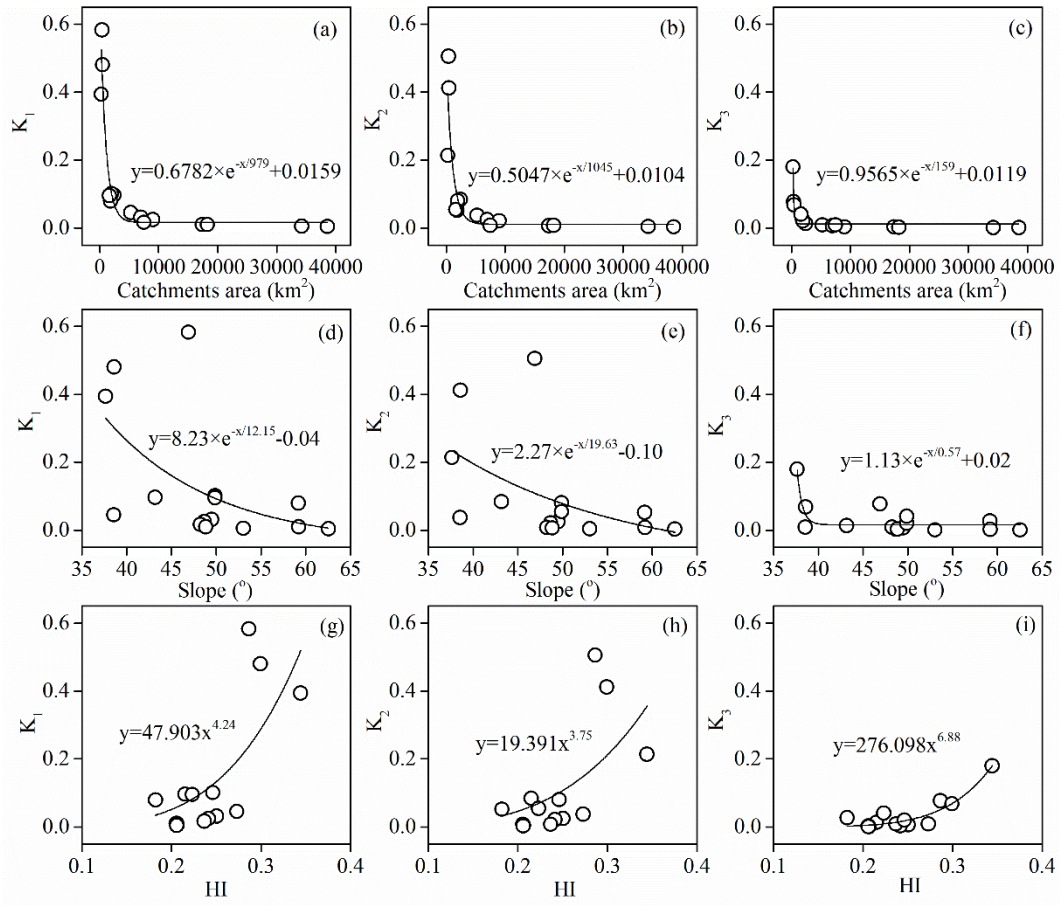

455

456 **Fig. 11 The relationships between K values and catchments area (a, b, c), average slope (d, e, f)**

457 **and HI (g, h, i) for the Beijiang River.**

458 **5.2 Temporary and net sink of atmospheric CO_2**

459 **5.2.1 Sulfate origin and DIC apportionment**

460 The successful application of DIC apportionment calculation mentioned in section 3.2.2 is

461 depended on the origions of sulfate (SO_4^{2-}). Three origions of SO_4^{2-} should be discriminated

462 including atmospheric acid deposition (Larssen and Carmichael, 2000), acid mining discharge

463 (AMD) (Li et al., 2018; Li et al., 2019) and chemical weathering of evaporite such as the dissolution

464 of gypsum (Appelo and Postma, 2005). Acid rain events occurred frequently in South and East

465 China after 1980 (Larssen et al., 2006). The pH isolines based on data from 86 monitoring stations

466 (Larssen et al., 2006) showed that in the Beijiang River the rain pH was lower than 4.5 and our

467 monitoring dataset also proved this result. Sulfur wet deposition estimated based on the observed

bulk wet sulfur deposition data and the RAINS-Asia model (Larssen and Carmichael, 2000) ranged from 2000-5000 eq ha^{-1} a^{-1}, which showed that the acid sulfur deposition was one of the most important sources of river sulfate. In addition, considering the abundant ore resources in the Beijiang River, the second possible source of SO_4^{2-} is sulfide oxidation due to mining. In our previous study, the SO_4^{2-} with AMD origin mainly came from the tributary Wenjiang River (Wen et al., 2018). These two sources could offer sufficient chemical weathering agent H_2SO_4 and actively involved in the chemical weathering due to the following reaction mechanism (take carbonate for example) (Taylor et al., 1984; van Everdingen and Krouse, 1985).

$$FeS_2 + \frac{7}{2}O_2 + H_2O = Fe^{2+} + 2SO_4^{2-} + 2H^+ \quad (35)$$

$$2CaCO_3 + H_2SO_4 = 2Ca^{2+} + 2HCO_3^- + SO_4^{2-} \quad (36)$$

The third source came from dissolution of gypsum could not offer active H_2SO_4 to induce carbonate and silicate dissolution. Two evidences were summarized to indicate the absence of gypsum in the study area, (1) Lithology in the river basin is composed of limestone, sandstone, gneiss and glutenite. HI showed that geomorphology development has entered into the “old” age, the evaporite such as halite and gypsum has been consumed by the dissolution. (2) The stoichiometric relationship between Ca^{2+} and SO_4^{2-} (Fig. 2) showed that all of the samples in the study area located below the 1:1 gypsum dissolution line, and they also below the 1:2 carbonate weathering induced by sulfuric acid (SCW) line. These two points combined gave the evidence to prove the absence of contribution of gypsum dissolution to river SO_4^{2-}. So that, the DIC apportionment could be calculated according to equation (18) to (21) and the result of three main processes (CCW, CSW and SCW) contributing to the DIC origin in the Beijiang River water are showed in Table 4. It was found that CCW was the dominant origin of DIC (35%~87%) and that

SCW (3%~15%) and CSW (7%~59%) were non-negligible weathering processes.

5.2.2 Temporary and net CO_2 sink

According to the classical view of the global carbon cycling (Berner and Kothavala, 2001), the CO_2 sink induced by chemical weathering varies for different time scales. At short-term timescale, carbonic acid based carbonate and silicate weathering (CCW and CSW) and transport of the HCO_3^- to oceans through rivers is an important "temporary" carbon sink (Khadka et al., 2014) and can be calculated by the sum of CCR_{CCW} and CCR_{CSW}. Thus, it was significant to estimate the CCR of CCW and CSW (Liu and Dreybrodt, 2015; Liu et al., 2011). However, at the geological timescale (>10^6 years), when over the timescale typical of residence time of HCO_3^- in the ocean (10^5 years), the CCW is not a mechanism that can participate in the net sink of CO_2 in the atmosphere because all of the atmospheric CO_2 fixed through CCW is returned to the atmosphere during carbonate precipitation in the ocean. Meanwhile, in case of CSW, followed by carbonate deposition, one of the two moles of CO_2 involved is transferred from the atmosphere to the lithosphere in the form of carbonate rocks, while the other one returns to the atmosphere. The CSW is recognized as the net sink of atmosphere CO_2. In addition, when sulfuric acid is involved as a proton donor in carbonate weathering, half of the carbon dissolved to the atmospheric during carbonate precipitation. Thus, SCW leads to a net release of CO_2 in ocean-atmosphere system. So that the net CO_2 sink (expressed by CCR_{Net} in this study) is controlled by the DIC apportionment according to equation (31).

The results of CCR_{Total}, CCR_{CCW}, CCR_{CSW} and CCR_{Net} were summarized in Table 4. The CCR_{Total} was 823.41 10^3 mol km^{-2} a^{-1}. Comparing with other Chinese rivers, such as the Songhua River (189×10^3 mol km^{-2} a^{-1}) (Cao et al., 2015) and other rivers calculated by (Gaillardet et al.,

1999) including the Heilong River (53×10^3 mol km^{-2} a^{-1}), the Changjiang River (609×10^3 mol km^{-2} a^{-1}), the Huanghe River (360×10^3 mol km^{-2} a^{-1}), the Xijiang River (960×10^3 mol km^{-2} a^{-1}), the Jinshajiang River (420×10^3 mol km^{-2} a^{-1}), the Langcangjiang River (980×10^3 mol km^{-2} a^{-1}), the Nujiang River (1240×10^3 mol km^{-2} a^{-1}), the Yalongjiang River (870×10^3 mol km^{-2} a^{-1}), the Daduhe River (1280×10^3 mol km^{-2} a^{-1}) and Minjiang River (660×10^3 mol km^{-2} a^{-1}), our study area showed relative high CCR due to high chemical weathering rate. In addition, the CCR_{CCW} and CCR_{CSW} were 536.59×10^3 (65%) and 286.82×10^3 (35%) mol km^{-2} a^{-1}, respectively. Compared with the "temporary" sink, the net sink of CO_2 for the Beijiang River was approximately 23.18×10^3 mol km^{-2} a^{-1} of CO_2 sinking in the perspective of global carbon cycling. It was about 3% of the "temporary" CO_2 sink. In addition, the CO_2 net sink of each sub basin were also different and show large spatial variations due to heterogeneity of geology and human activities. The geology showed weak correlation with the CO_2 net sink (Fig. 12a), while the $[SO_4^{2-}]_{SCW}$ and $[SO_4^{2-}]_{SSW}$ have weak negative correlation with the CO_2 net sink (Fig. 12b). It proved that human activities (sulfur acid deposition and AMD) decreased the CO_2 net sink and even make chemical weathering a CO_2 source to the atmosphere.

Table 4 Calculated CO_2 consumption rate and net sink of 15 nested subcatchments in the Beijiang River Basin

Hydrological stations	DIC apportionment (10^9 mol a^{-1})			"Temporary" Sink (CO_2 consumption rate) (10^3 mol km^{-2} a^{-1})			Net Sink (10^3 mol km^{-2} a^{-1})
	CCW	SCW	CSW	CCR_{CCW}	CCR_{CSW}	CCR_{Total}	CCR_{Net}
JLWs	0.10	0.00	0.05	175.23	191.14	366.36	87.73
CXs	0.57	0.04	0.05	732.05	118.18	850.23	13.18
HJTs	1.57	0.06	0.34	1563.64	683.41	2247.05	286.14
ZKs	1.24	0.16	0.73	375.23	439.77	815.00	172.27
XGLs	0.85	0.14	0.37	227.05	195.91	422.95	61.59

WJs	1.76	0.17	0.87	449.32	443.18	892.50	177.50
LXs	7.30	0.40	2.61	1485.45	1060.45	2545.91	449.09
LCs	8.07	0.86	1.92	764.32	363.41	1127.95	99.77
LSs	10.13	0.42	2.48	724.55	354.32	1078.64	147.05
XSs	2.08	0.41	3.52	138.64	469.09	607.73	207.05
GDs	16.48	0.71	7.60	912.73	841.82	1754.55	381.36
SKs	4.00	0.72	1.74	114.77	100.23	215.00	29.55
YDs	14.11	1.75	13.10	386.82	718.64	1105.45	311.14
FLXs	40.38	7.74	4.46	589.77	130.45	720.23	-47.73
SJs	41.36	9.27	11.05	536.59	286.82	823.41	23.18

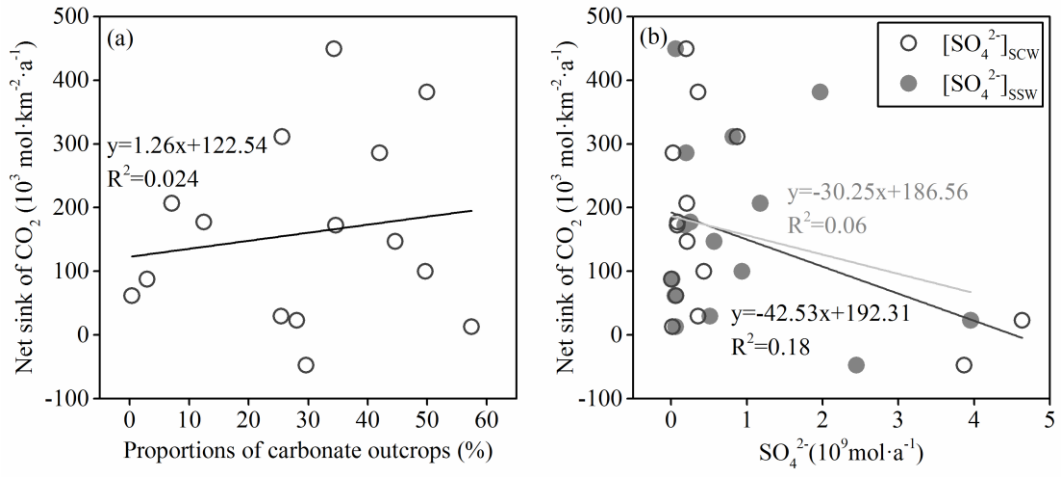

Fig. 12 Correlations between CO_2 net sinks and proportions of proportions of carbonate (a) and correlations between CO_2 net sinks and $[SO_4^{2-}]_{SCW}$ or $[SO_4^{2-}]_{SSW}$ (b)

6 Conclusions

This study revealed the temporary and net sinks of atmospheric CO_2 due to chemical weathering in a subtropical hyperactive catchment with mixing carbonate and silicate lithology under the stress of chemical weathering induced by anthropogenic sulfuric acid agent. During the sampling period, the pH values ranged from 7.5 to 8.5 and TDS varied from 73.8 to 230.2 $mg \cdot L^{-1}$. Ca^{2+} and HCO_3^- were the dominated cation and anion. Water chemical patterns and PCA showed that carbonate and silicate weathering were the most important processes controlling the local

hydrochemistry. In average, carbonate and silicate weathering contributed approximately 50.06% and 25.71% of the total cationic loads, respectively.

The average of carbonate and silicate weathering rate in the Beijiang River Basin were 61.15 and 25.31 $t \cdot km^{-2} \cdot a^{-1}$, respectively. The high rate was comparable to other rivers located in the hyperactive zone between the latitude 0-30°. The lithology, runoff and geomorphology had significant influences on the chemical weathering rate. (1) Due to the difference between kinetics of carbonate and silicate dissolution processes, the proportion of carbonate outcrops had significant positive correlation with the chemical weathering rate and confirmed that carbonate outcrops ratios was the sensitive factor controlling the chemical weathering rates and the rapid kinetics of carbonate dissolution played an important role in weathering rates. (2) Runoff mainly controlled the season variations and the dilution effect was weak in the study area. Due to the compensation effect of chemical weathering, significant positive linear relationship was detected between Q and TWR, CWR and SWR. (3) The geomorphology factors such as slope and HI had non-linear correlation on chemical weathering rate and showed significant scale effect, which revealed the complexity in chemical weathering processes.

DIC apportionment showed that CCW was the dominant origin of DIC (35%-87%) and that SCW (3%-15%) and CSW (7%-59%) were non-negligible weathering processes. The CCR_{Total} was 823.41 10^3 mol km^{-2} a^{-1}, relative high CCR due to high chemical weathering rate. In addition, the CCR_{CCW} and CCR_{CSW} were 536.59×10^3 (65%) and 286.82×10^3 (35%) mol km^{-2} a^{-1}, respectively. Compared with the "temporary" sink, the net sink of CO_2 for the Beijiang River was approximately 23.18×10^3 mol km^{-2} a^{-1} of CO_2 sinking in the perspective of global carbon cycling. It was about 2.82% of the "temporary" CO_2 sink. Human activities such as sulfur acid deposition and AMD have

562 significantly altered the CO_2 sinks.

563 **7 Acknowledgments**

564 This research work was financially supported by the General Program of the National Natural
565 Science Foundation of China (No.41877470), the Natural Science Foundation of Guangdong
566 Province, China (No. 2017A030313231) and the Natural Science Foundation of Guangdong
567 Province, China (No. 2017A030313229).

568 **8 Code/Data availability:** Yes.

569 **9 Author contribution:** Cao Yingjie and Tang Changyuan designed the study, carried out the
570 field work, analyzed the results, and drafted the manuscript. Xuan Yingxue and Guan Shuai
571 participated in the field sampling and laboratory analysis. Peng Yisheng reviewed and edited the
572 original draft of the manuscript. All authors read and approved the final manuscript.

573 **10 Competing interests:** No.

574 **References**

575 Appelo, C. A. J., and Postma, D.: Geochemistry, groundwater and pollution, CRC press, 2005.
576 Berner, R. A., and Kothavala, Z.: GEOCARB III: a revised model of atmospheric CO_2 over
577 Phanerozoic time, American Journal of Science, 301, 182-204, 0002-9599, 2001.
578 Cao, Y., Tang, C., Song, X., and Liu, C.: Major ion chemistry, chemical weathering and CO_2
579 consumption in the Songhua River basin, Northeast China, Environmental Earth Sciences, 73,
580 7505-7516, 2015.
581 Cao, Y., Tang, C., Cao, G., and Wang, X.: Hydrochemical zoning: natural and anthropogenic origins
582 of the major elements in the surface water of Taizi River Basin, Northeast China,
583 Environmental Earth Sciences, 75, 1-14, 2016b.
584 Chen, J., Wang, F., Xia, X., and Zhang, L.: Major element chemistry of the Changjiang (Yangtze
585 River), Chemical Geology, 187, 231-255, 2002.
586 Chen, J., Wang, F., Meybeck, M., He, D., Xia, X., and Zhang, L.: Spatial and temporal analysis of
587 water chemistry records (1958–2000) in the Huanghe (Yellow River) basin, Global
588 biogeochemical cycles, 19, 2005.
589 Ding, H., Liu, C.-Q., Zhao, Z.-Q., Li, S.-L., Lang, Y.-C., Li, X.-D., Hu, J., and Liu, B.-J.:
590 Geochemistry of the dissolved loads of the Liao River basin in northeast China under
591 anthropogenic pressure: Chemical weathering and controlling factors, Journal of Asian Earth
592 Sciences, 138, 657-671, https://doi.org/10.1016/j.jseaes.2016.07.026, 2017.
593 Donnini, M., Frondini, F., Probst, J.-L., Probst, A., Cardellini, C., Marchesini, I., and Guzzetti, F.:
594 Chemical weathering and consumption of atmospheric carbon dioxide in the Alpine region,

595 Global and Planetary Change, 136, 65-81, https://doi.org/10.1016/j.gloplacha.2015.10.017,
596 2016.
597 Dosseto, A., Bourdon, B., Gaillardet, J., Allègre, C. J., and Filizola, N.: Time scale and conditions
598 of weathering under tropical climate: Study of the Amazon basin with U-series, Geochimica et
599 Cosmochimica Acta, 70, 71-89, https://doi.org/10.1016/j.gca.2005.06.033, 2006.
600 Edmond, J. M., Palmer, M. R., Measures, C. I., Brown, E. T., and Huh, Y.: Fluvial geochemistry of
601 the eastern slope of the northeastern Andes and its foredeep in the drainage of the Orinoco in
602 Colombia and Venezuela, Geochimica et Cosmochimica Acta, 60, 2949-2974,
603 https://doi.org/10.1016/0016-7037(96)00142-1, 1996.
604 Eiriksdottir, E. S., Gislason, S. R., and Oelkers, E. H.: Does runoff or temperature control chemical
605 weathering rates?, Applied Geochemistry, 26, S346-S349,
606 https://doi.org/10.1016/j.apgeochem.2011.03.056, 2011.
607 Fernandes, A. M., Conceição, F. T. d., Spatti Junior, E. P., Sardinha, D. d. S., and Mortatti, J.:
608 Chemical weathering rates and atmospheric/soil CO_2 consumption of igneous and
609 metamorphic rocks under tropical climate in southeastern Brazil, Chemical Geology, 443, 54-
610 66, https://doi.org/10.1016/j.chemgeo.2016.09.008, 2016.
611 Gaillardet, J., Dupré, B., Louvat, P., and Allègre, C. J.: Global silicate weathering and CO_2
612 consumption rates deduced from the chemistry of large rivers, Chemical Geology, 159, 3-30,
613 https://doi.org/10.1016/S0009-2541(99)00031-5, 1999.
614 Galy, A., and France-Lanord, C.: Weathering processes in the Ganges–Brahmaputra basin and the
615 riverine alkalinity budget, Chemical Geology, 159, 31-60, https://doi.org/10.1016/S0009-
616 2541(99)00033-9, 1999.
617 Gao, Q., Tao, Z., Huang, X., Nan, L., Yu, K., and Wang, Z.: Chemical weathering and CO2
618 consumption in the Xijiang River basin, South China, Geomorphology, 106, 324-332,
619 https://doi.org/10.1016/j.geomorph.2008.11.010, 2009.
620 Garrels, R. M.: The carbonate-silicate geochemical cycle and its effect on atmospheric carbon
621 dioxide over the past 100 million years, Am J Sci, 283, 641-683, 1983.
622 Gibbs, R. J.: Water chemistry of the Amazon River, Geochimica et Cosmochimica Acta, 36, 1061-
623 1066, https://doi.org/10.1016/0016-7037(72)90021-X, 1972.
624 Gislason, S. R., Oelkers, E. H., Eiriksdottir, E. S., Kardjilov, M. I., Gisladottir, G., Sigfusson, B.,
625 Snorrason, A., Elefsen, S., Hardardottir, J., Torssander, P., and Oskarsson, N.: Direct evidence
626 of the feedback between climate and weathering, Earth and Planetary Science Letters, 277,
627 213-222, https://doi.org/10.1016/j.epsl.2008.10.018, 2009.
628 Guo, J., Wang, F., Vogt, R. D., Zhang, Y., and Liu, C. Q.: Anthropogenically enhanced chemical
629 weathering and carbon evasion in the Yangtze Basin, Scientific Reports, 5, 11941, 2015.
630 Hagedorn, B., and Cartwright, I.: Climatic and lithologic controls on the temporal and spatial
631 variability of CO_2 consumption via chemical weathering: An example from the Australian
632 Victorian Alps, Chemical Geology, 260, 234-253,
633 https://doi.org/10.1016/j.chemgeo.2008.12.019, 2009.
634 Hartmann, J., Jansen, N., Dürr, H. H., Kempe, S., and Köhler, P.: Global CO_2-consumption by
635 chemical weathering: What is the contribution of highly active weathering regions?, Global
636 and Planetary Change, 69, 185-194, https://doi.org/10.1016/j.gloplacha.2009.07.007, 2009.
637 Hartmann, J., Moosdorf, N., Lauerwald, R., Hinderer, M., and West, A. J.: Global chemical
638 weathering and associated P-release - The role of lithology, temperature and soil properties,

Chemical Geology, 363, 145-163, https://doi.org/10.1016/j.chemgeo.2013.10.025, 2014a.
Hartmann, J., West, J., Renforth, P., Köhler, P., Rocha, C. D. L., Wolf-Gladrow, D., Dürr, H., and Scheffran, J.: Enhanced chemical weathering as a sink for carbon dioxide, a nutrient source and a strategy to mitigate ocean acidification, Reviews of Geophysics, 2014b.
He Jiangyi, Z. D., Zhao zhiqi: Spatial and temporal variations in hydrochemical composition of river water in Yellow River Basin, China, Chinese Journal of Ecology, 1-12, 2017.
Hercod, D. J., Brady, P. V., and Gregory, R. T.: Catchment-scale coupling between pyrite oxidation and calcite weathering, Chemical Geology, 151, 259-276, https://doi.org/10.1016/S0009-2541(98)00084-9, 1998.
Huh, Y., and Edmond, J. M.: The fluvial geochemistry of the rivers of Eastern Siberia: III. Tributaries of the Lena and Anabar draining the basement terrain of the Siberian Craton and the Trans-Baikal Highlands, Geochimica et Cosmochimica Acta, 63, 967-987, https://doi.org/10.1016/S0016-7037(99)00045-9, 1999.
Jiang, H., Liu, W., Xu, Z., Zhou, X., Zheng, Z., Zhao, T., Zhou, L., Zhang, X., Xu, Y., and Liu, T.: Chemical weathering of small catchments on the Southeastern Tibetan Plateau I: Water sources, solute sources and weathering rates, Chemical Geology, 500, 159-174, https://doi.org/10.1016/j.chemgeo.2018.09.030, 2018.
Kempe, S., and Degens, E. T.: An early soda ocean?, Chemical Geology, 53, 95-108, https://doi.org/10.1016/0009-2541(85)90023-3, 1985.
Khadka, M. B., Martin, J. B., and Jin, J.: Transport of dissolved carbon and CO_2 degassing from a river system in a mixed silicate and carbonate catchment, Journal of Hydrology, 513, 391-402, https://doi.org/10.1016/j.jhydrol.2014.03.070, 2014.
Larssen, T., and Carmichael, G. R.: Acid rain and acidification in China: the importance of base cation deposition, Environmental Pollution, 110, 89-102, https://doi.org/10.1016/S0269-7491(99)00279-1, 2000.
Larssen, T., Lydersen, E., Tang, D., He, Y., Gao, J., Liu, H., Duan, L., Seip, H. M., Vogt, R. D., Mulder, J., Shao, M., Wang, Y., Shang, H., Zhang, X., Solberg, S., Aas, W., Okland, T., Eilertsen, O., Angell, V., Li, Q., Zhao, D., Xiang, R., Xiao, J., and Luo, J.: Acid Rain in China, Environmental Science & Technology, 40, 418-425, 10.1021/es0626133, 2006.
Lenton, T. M., and Britton, C.: Enhanced carbonate and silicate weathering accelerates recovery from fossil fuel CO2 perturbations, Global Biogeochemical Cycles, 20, 10.1029/2005gb002678, 2006.
Li, R., Tang, C., Cao, Y., Jiang, T., and Chen, J.: The distribution and partitioning of trace metals (Pb, Cd, Cu, and Zn) and metalloid (As) in the Beijiang River, Environmental Monitoring and Assessment, 190, 399, 10.1007/s10661-018-6789-x, 2018.
Li, R., Tang, C., Li, X., Jiang, T., Shi, Y., and Cao, Y.: Reconstructing the historical pollution levels and ecological risks over the past sixty years in sediments of the Beijiang River, South China, Science of The Total Environment, 649, 448-460, https://doi.org/10.1016/j.scitotenv.2018.08.283, 2019.
Li, S. L., Calmels, D., Han, G., Gaillardet, J., and Liu, C. Q.: Sulfuric acid as an agent of carbonate weathering constrained by $\delta^{13}C_{DIC}$: Examples from Southwest China, Earth and Planetary Science Letters, 270, 189-199, https://doi.org/10.1016/j.epsl.2008.02.039, 2008.
Li, S., Lu, X. X., He, M., Zhou, Y., Bei, R., Li, L., and Ziegler, A. D.: Major element chemistry in the upper Yangtze River: A case study of the Longchuanjiang River, Geomorphology, 129, 29-

683 42, https://doi.org/10.1016/j.geomorph.2011.01.010, 2011.
684 Li, S., Lu, X. X., and Bush, R. T.: Chemical weathering and CO_2 consumption in the Lower Mekong
685 River, Science of The Total Environment, 472, 162-177,
686 https://doi.org/10.1016/j.scitotenv.2013.11.027, 2014.
687 Liu, B., Liu, C.-Q., Zhang, G., Zhao, Z.-Q., Li, S.-L., Hu, J., Ding, H., Lang, Y.-C., and Li, X.-D.:
688 Chemical weathering under mid- to cool temperate and monsoon-controlled climate: A study
689 on water geochemistry of the Songhuajiang River system, northeast China, Applied
690 Geochemistry, 31, 265-278, https://doi.org/10.1016/j.apgeochem.2013.01.015, 2013.
691 Liu, Z., Dreybrodt, W., and Liu, H.: Atmospheric CO_2 sink: Silicate weathering or carbonate
692 weathering?, Applied Geochemistry, 26, S292-S294,
693 https://doi.org/10.1016/j.apgeochem.2011.03.085, 2011.
694 Liu, Z., and Dreybrodt, W.: Significance of the carbon sink produced by H_2O–carbonate–CO_2–
695 aquatic phototroph interaction on land, Science Bulletin, 60, 182-191, 2095-9273, 2015.
696 Ludwig, W., Amiotte-Suchet, P., Munhoven, G., and Probst, J.-L.: Atmospheric CO2 consumption
697 by continental erosion: present-day controls and implications for the last glacial maximum,
698 Global and Planetary Change, 16-17, 107-120, https://doi.org/10.1016/S0921-8181(98)00016-
699 2, 1998.
700 Meybeck, M., Dürr, H. H., and Vörösmarty, C. J.: Global coastal segmentation and its river
701 catchment contributors: A new look at land-ocean linkage, Global Biogeochemical Cycles, 20,
702 10.1029/2005gb002540, 2006.
703 Mora, A., Baquero, J. C., Alfonso, J. A., Pisapia, D., and Balza, L.: The Apure River: geochemistry
704 of major and selected trace elements in an Orinoco River tributary coming from the Andes,
705 Venezuela, Hydrological Processes, 24, 3798-3810, 10.1002/hyp.7801, 2010.
706 Mortatti, J., and Probst, J.-L.: Silicate rock weathering and atmospheric/soil CO2 uptake in the
707 Amazon basin estimated from river water geochemistry: seasonal and spatial variations,
708 Chemical Geology, 197, 177-196, https://doi.org/10.1016/S0009-2541(02)00349-2, 2003.
709 Négrel, P., Allègre, C. J., Dupré, B., and Lewin, E.: Erosion sources determined by inversion of
710 major and trace element ratios and strontium isotopic ratios in river water: The Congo Basin
711 case, Earth and Planetary Science Letters, 120, 59-76, https://doi.org/10.1016/0012-
712 821X(93)90023-3, 1993.
713 Ollivier, P., Hamelin, B., and Radakovitch, O.: Seasonal variations of physical and chemical erosion:
714 A three-year survey of the Rhone River (France), Geochimica et Cosmochimica Acta, 74, 907-
715 927, https://doi.org/10.1016/j.gca.2009.10.037, 2010.
716 Pike, R. J., and WILSON, S. E.: Elevation-Relief Ratio, Hypsometric Integral, and Geomorphic
717 Area-Altitude Analysis, GSA Bulletin, 82, 1079-1084, 10.1130/0016-
718 7606(1971)82[1079:erhiag]2.0.co;2, 1971.
719 Ran, X., Yu, Z., Yao, Q., Chen, H., and Mi, T.: Major ion geochemistry and nutrient behaviour in
720 the mixing zone of the Changjiang (Yangtze) River and its tributaries in the Three Gorges
721 Reservoir, Hydrological processes, 24, 2481-2495, 2010.
722 Rao, W., Zheng, F., Tan, H., Yong, B., Jin, K., Wang, S., Zhang, W., Chen, T., and Wang, Y.: Major
723 ion chemistry of a representative river in South-central China: Runoff effects and controlling
724 mechanisms, Journal of Hazardous Materials, 378, 120755,
725 https://doi.org/10.1016/j.jhazmat.2019.120755, 2019.
726 Ryu, J. S., Lee, K. S., Chang, H.-W., and Shin, H. S.: Chemical weathering of carbonates and

727 silicates in the Han River basin, South Korea, Chemical Geology, 247, 66-80,
728 https://doi.org/10.1016/j.chemgeo.2007.09.011, 2008.
729 Singh, O., Sarangi, A., and Sharma, M. C.: Hypsometric Integral Estimation Methods and its
730 Relevance on Erosion Status of North-Western Lesser Himalayan Watersheds, Water
731 Resources Management, 22, 1545-1560, 10.1007/s11269-008-9242-z, 2008.
732 Spence, J., and Telmer, K.: The role of sulfur in chemical weathering and atmospheric CO_2 fluxes:
733 Evidence from major ions, $\delta^{13}C_{DIC}$, and $\delta^{34}S_{SO4}$ in rivers of the Canadian Cordillera,
734 Geochimica et Cosmochimica Acta, 69, 5441-5458, https://doi.org/10.1016/j.gca.2005.07.011,
735 2005.
736 Stallard, R. F., and Edmond, J. M.: Geochemistry of the Amazon: 1. Precipitation chemistry and the
737 marine contribution to the dissolved load at the time of peak discharge, Journal of Geophysical
738 Research: Oceans, 86, 9844-9858, 10.1029/JC086iC10p09844, 1981.
739 Stallard, R. F., and Edmond, J. M.: Geochemistry of the Amazon: 2. The influence of geology and
740 weathering environment on the dissolved load, Journal of Geophysical Research: Oceans, 88,
741 9671-9688, 10.1029/JC088iC14p09671, 1983.
742 Stallard, R. F., and Edmond, J. M.: Geochemistry of the Amazon: 3. Weathering chemistry and limits
743 to dissolved inputs, Journal of Geophysical Research: Oceans, 92, 8293-8302,
744 10.1029/JC092iC08p08293, 1987.
745 STRAHLER, A. N.: HYPSOMETRIC (AREA-ALTITUDE) ANALYSIS OF EROSIONAL
746 TOPOGRAPHY, GSA Bulletin, 63, 1117-1142, 10.1130/0016-
747 7606(1952)63[1117:haaoet]2.0.co;2, 1952.
748 Sun, X., Mörth, C.-M., Humborg, C., and Gustafsson, B.: Temporal and spatial variations of rock
749 weathering and CO2 consumption in the Baltic Sea catchment, Chemical Geology, 466, 57-69,
750 https://doi.org/10.1016/j.chemgeo.2017.04.028, 2017.
751 Taylor, B. E., Wheeler, M. C., and Nordstrom, D. K.: Stable isotope geochemistry of acid mine
752 drainage: Experimental oxidation of pyrite, Geochimica et Cosmochimica Acta, 48, 2669-2678,
753 https://doi.org/10.1016/0016-7037(84)90315-6, 1984.
754 Van Everdingen, R. O., and Krouse, H. R.: Isotope composition of sulphates generated by bacterial
755 and abiological oxidation, Nature, 315, 395-396, 10.1038/315395a0, 1985.
756 Viers, J., Oliva, P., Dandurand, J. L., Dupré, B., and Gaillardet, J.: Chemical weathering rates, CO2
757 consumption, and control parameters deduced from the chemical composition of rivers, 2014.
758 Walling, D. E.: Solute in river systems, Solute Processes, 251-327, 1986.
759 Wen, J., Tang, C., Cao, Y., Li, X., and Chen, Q.: Hydrochemical evolution of groundwater in a
760 riparian zone affected by acid mine drainage (AMD), South China: the role of river–
761 groundwater interactions and groundwater residence time, Environmental Earth Sciences, 77,
762 794, 10.1007/s12665-018-7977-2, 2018.
763 Wu, W., Xu, S., Yang, J., and Yin, H.: Silicate weathering and CO_2 consumption deduced from the
764 seven Chinese rivers originating in the Qinghai-Tibet Plateau, Chemical Geology, 249, 307-
765 320, 2008.
766 Xie chenji, G. Q., Tao zhen, Liu Longhai, Lishanchi: Chemical weathering and CO_2 consumption
767 in the Dongjiang River Basin, Acta Scientiae Circumstantiae, 33, 2123-2133, 2013.
768 Xiong, L., Tang, G., Yuan, B., Lu, Z., Li, F., and Zhang, L.: Geomorphological inheritance for loess
769 landform evolution in a severe soil erosion region of Loess Plateau of China based on digital
770 elevation models, Science China Earth Sciences, 57, 1944-1952, 10.1007/s11430-014-4833-4,

771 2014.
772 Xu, Z., and Liu, C.-Q.: Water geochemistry of the Xijiang basin rivers, South China: Chemical
773 weathering and CO_2 consumption, Applied Geochemistry, 25, 1603-1614, 2010.
774 Zeng, C., Liu, Z., Zhao, M., and Yang, R.: Hydrologically-driven variations in the karst-related
775 carbon sink fluxes: Insights from high-resolution monitoring of three karst catchments in
776 Southwest China, Journal of Hydrology, 533, 74-90,
777 https://doi.org/10.1016/j.jhydrol.2015.11.049, 2016.
778 Zhang, J., Huang, W., Letolle, R., and Jusserand, C.: Major element chemistry of the Huanghe
779 (Yellow River), China-weathering processes and chemical fluxes, Journal of Hydrology, 168,
780 173-203, 1995.
781 Zhang, L., Song, X., Xia, J., Yuan, R., Zhang, Y., Liu, X., and Han, D.: Major element chemistry of
782 the Huai River basin, China, Applied Geochemistry, 26, 293-300, 2011.
783 Zhang, S. R., Lu, X. X., Higgitt, D. L., Chen, C. T. A., Sun, H. G., and Han, J. T.: Water chemistry
784 of the Zhujiang (Pearl River): natural processes and anthropogenic influences. Journal of
785 Geophysical Research, 112(F1), F01011, Journal of Geophysical Research Atmospheres, 112,
786 137-161, 2007.

787 **Supplementary material**

788 **Table S1 The major ions concentrations of rain water samples at 5 hydrological stations in the**

789 **Beijiang River (mean±SD).**

Hydrological stations	Na^+ (μmol/L)	K^+ (μmol/L)	Ca^{2+} (μmol/L)	Mg^{2+} (μmol/L)	Cl^- (μmol/L)	SO_4^{2-} (μmol/L)	NO_3^- (μmol/L)
XGLs	12.8±9.7	21.0±16.8	22.2±20.5	10.9±10.3	25.9±22.6	320.2±370.7	83.3±85.2
XSs	20.4±11.8	7.8±4.5	86.9±30.4	10.1±5.2	10.0±0.0	606.5±511.5	36.3±23.4
Yds	16.3±9.5	10.1±10.8	161.1±56.5	9.0±7.8	23.9±12.4	136.9±169.5	143.1±135.5
FLXs	18.8±12.3	3.2±2.5	31.1±17.7	4.2±2.7	23.1±16.6	45.4±27.5	77.1±70.4
SJs	12.6±9.2	12.5±16.3	22.9±13.8	15.4±18.1	25.4±16.0	79.0±79.8	156.7±206.4

790